

Hydrodynamical simulations and semi-analytic models of galaxy formation: two sides of the same coin

Eyal Neistein,^{*1} Sadegh Khochfar,¹ Claudio Dalla Vecchia,¹ Joop Schaye²

¹ *Max-Planck-Institute for Extraterrestrial Physics, Giessenbachstrasse 1, 85748 Garching, Germany*

² *Leiden Observatory, Leiden University, P.O. Box 9513, 2300 RA Leiden, the Netherlands*

ABSTRACT

In this work we develop a new method to turn a state-of-the-art hydrodynamical cosmological simulation of galaxy formation (HYD) into a simple semi-analytic model (SAM). This is achieved by summarizing the efficiencies of accretion, cooling, star formation, and feedback given by the HYD, as functions of the halo mass and redshift. The SAM then uses these functions to evolve galaxies within merger-trees that are extracted from the same HYD. Surprisingly, by turning the HYD into a SAM, we conserve the mass of individual galaxies, with deviations at the level of 0.1 dex, on an object-by-object basis, with no significant systematics. This is true for all redshifts, and for the mass of stars and gas components, although the agreement reaches 0.2 dex for satellite galaxies at low redshift. We show that the same level of accuracy is obtained even in case the SAM uses only one phase of gas within each galaxy. Moreover, we demonstrate that the formation history of one massive galaxy provides sufficient information for the SAM to reproduce the population of galaxies within the entire cosmological box. The reasons for the small scatter between the HYD and SAM galaxies are: a) The efficiencies are matched as functions of the halo mass and redshift, meaning that the evolution within merger-trees agrees on average. b) For a given galaxy, efficiencies fluctuate around the mean value on time scales of 0.2–2 Gyr. c) The various mass components of galaxies are obtained by integrating the efficiencies over time, averaging out these fluctuations. We compare the efficiencies found here to standard SAM recipes and find that they often deviate significantly. For example, here the HYD shows smooth accretion that is less effective for low mass haloes, and is always composed of hot or dilute gas; cooling is less effective at high redshift; and star formation changes only mildly with cosmic time. The method developed here can be applied in general to any HYD, and can thus serve as a common language for both HYDs and SAMs.

Key words: galaxies: evolution - galaxies: formation - galaxies: haloes - large-scale structure of Universe.

1 INTRODUCTION

The formation and evolution of galaxies within our Universe is a complicated process that combines two very different mechanisms. On the one hand, the hierarchical growth of dark-matter structure drives the aggregation of galaxies, on time-scales that are proportional to redshift (Press & Schechter 1974; Lacey & Cole 1993). On the other hand, the baryonic physics determines the interplay between gas and stars, on time scales that are affected by local processes of cooling, star formation (SF) and feedback (White & Rees 1978; Dekel & Silk 1986; White & Frenk 1991; McKee & Ostriker 2007). The combination of these two disciplines shapes the complex evolution of galaxies over cosmic time.

Models that take into account the above processes differ in

their level of complexity, and in the typical scales that are being resolved or properly modeled. In general, a simple distinction can be made between two different approaches, namely hydrodynamical simulations (hereafter HYDs), and semi-analytic models (SAMs). HYDs try to follow the evolution of a galaxy, by modelling in great detail the hydrodynamics and gravitation laws that are in play. These models often use more than 10^6 particles to describe one galaxy, and thus allow its detailed structure to be explored. However, HYDs are still limited to a finite resolution, which does not allow all the processes mentioned above to be followed properly. Consequently, HYDs rely on ‘sub-grid’ analytical laws, that describe SF, feedback, and the structure of the inter-stellar medium (ISM). For a few examples of HYD studies, see Katz et al. (1996); Governato et al. (1999); Springel & Hernquist (2003); Scannapieco et al. (2009); Schaye et al. (2010); Agertz et al. (2011).

* E-mail: eyal@mpe.mpg.de

A different approach, adopted by SAMs, is to treat each galaxy as one unresolved object, using integrated properties to describe the mass of stars, cold gas, hot gas, and the black hole. Since each component of the galaxy is represented by one number, the dynamics within the galaxy is not resolved, and one needs to come up with laws for star formation, cooling, and feedback that are valid on average for the entire galaxy.¹ Due to their simplicity, SAMs can provide a statistical sample of galaxies, and can explore a large portion of their parameter space. For more details, the reader is referred to some recent SAM studies: Monaco et al. (2007); Somerville et al. (2008); Benson & Bower (2010); Guo et al. (2011); Wang et al. (2011); Khochfar et al. (2011).

In the last two decades, HYDs and SAMs have been used as the two major tools for studying the formation and evolution of galaxies. Detailed comparisons between the two approaches are thus important both for developing better models, and for having a common language to interpret different models. Following this reasoning, various comparisons between the two methods were made to date. Most of these studies have focused on the processes of accretion and cooling, finding some agreement at low redshift, and larger deviations at high- z . For more details, see Benson et al. (2001); Yoshida et al. (2002); Helly et al. (2003); Cattaneo et al. (2007); Viola et al. (2008); Saro et al. (2010); Lu et al. (2011); Hirschmann et al. (2011). In each of the above works, both the SAM and the HYD are adopting a specific model with a given parametrization. Thus, it is not clear if the discrepancies found between the HYD and SAM galaxies are due to the limitation of each methodology, or are just a simple outcome of the specific model chosen. A few other works have tried to quantify the physics of HYDs without using a SAM (e.g. Hernquist & Springel 2003; Rasera & Teysier 2006; Davé et al. 2011). Although such studies are important for understanding the physics of galaxy formation, it is difficult to estimate the accuracy of these models for individual objects.

Recently, Stringer et al. (2010) have tried a different path to attack this issue, by trying to tune a SAM according to the physics of a HYD. These authors managed to modify a SAM based on Bower et al. (2006), so that it will roughly reproduce the history of one disk galaxy within a HYD. Since their work was based on only one galaxy, and since some deviations between their SAM and the HYD remained, it is still not clear how well the two methodologies agree.

In this work we would like to take this approach one step further. We will develop a method to extract the physics of a HYD using the simulation output, in a way that can be used within a SAM. We use a large cosmological hydrodynamical simulation, based on state-of-the-art physical modelling, as developed by Schaye et al. (2010). Our task is to explore the level of complexity needed by a SAM in order to follow accurately the formation histories of galaxies as modeled by the HYD within a large cosmological box.

This paper is organized as follows. In section 2 we describe the HYD and the SAM used here, and the method being used to extract SAM ingredients out of the HYD. These ingredients are presented in section 3, emphasizing the differences in comparison to standard SAMs. The galaxies produced by both models are compared in section 4. A model with one gas phase is presented in section 5, showing a similar match to the HYD as in the case of the standard

SAM. In section 6 we further discuss a few additional tests of the formalism, and try to pin down the reasons for its success. Lastly, we summarize and discuss the results in section 7.

2 METHODS

2.1 The hydrodynamical simulation (HYD)

In this work we use a cosmological hydrodynamical simulation (HYD) based on the Overwhelmingly Large Simulations (OWLS) project (Schaye et al. 2010). This project includes a large set of HYDs with various different physical ingredients that were studied extensively by e.g. Sales et al. (2010); Wiersma et al. (2011); van de Voort et al. (2011); McCarthy et al. (2011). Here we only use one simulation setup, the same as the ‘reference model’ developed by Schaye et al. (2010). In brief, this model includes radiative cooling based on Wiersma et al. (2009), following the contributions from 11 different elements that are released by stellar winds from massive stars, AGB stars and by supernovae of types Ia and II, as described in Wiersma et al. (2009). The SF law is guided by the observed Kennicutt-Schmidt law, implemented in the form of a pressure law as described in Schaye & Dalla Vecchia (2008). Supernova (SN) feedback is modeled by injecting SN energy in kinetic form, following Dalla Vecchia & Schaye (2008). This model includes neither active galactic nuclei (AGN) nor black holes.

We ran a new simulation that is identical to the OWLS reference model with a box size of $100 h^{-1} \text{Mpc}$, and 2×512^3 particles of dark-matter, gas and stars. The simulation outputs were saved in 68 snapshots, more than the original run, and approximately spaced by 200 Myr, from $z = 20$ to $z = 0$. The dark-matter particle mass equals $4.06 \times 10^8 h^{-1} M_{\odot}$, and baryonic particles have initial mass of $8.66 \times 10^7 h^{-1} M_{\odot}$. The comoving (Plummer-equivalent) gravitational softening is $7.8 h^{-1} \text{kpc}$ (with a maximum value of $2 h^{-1} \text{kpc}$ in physical units). The underlying cosmological parameters are: $(\Omega_m, \sigma_8, n_s, \Omega_b, h) = (0.238, 0.74, 0.951, 0.0418, 0.73)$, consistent with the WMAP 5-year data (Komatsu et al. 2009).

On each output snapshot we have run the FOF algorithm with a linking length of 0.2 (Davis et al. 1985) to identify haloes with more than 20 dark-matter particles. The SUBFIND algorithm (Springel et al. 2001) was then used to identify subhaloes with more than 20 particles within haloes (i.e. the minimum subhalo mass ranges between 1×10^9 to $8 \times 10^9 h^{-1} M_{\odot}$, depending on which particles are included). In our implementation, SUBFIND uses both dark matter and baryonic particles (Dolag et al. 2009). Since satellite subhaloes within a dense environment are often being stripped of their dark-matter, subhaloes occasionally host only star and gas particles. In addition, fragmentation might happen within haloes, creating new subhaloes, with only gas and star particles. We have constructed merger-trees of subhaloes in the same way as described in Springel et al. (2001). The trees include information on the subhaloes and their host FOF groups.

2.2 The semi-analytic model (SAM)

Here we describe the semi-analytic model (SAM) used in this work. For more details on the model, including various specific scenarios for galaxy evolution, see Neistein & Weinmann (2010). The model follows galaxies inside the complex structure of merger-trees, and uses simple laws for cooling, SF, accretion, merging, and feedback. Unlike other SAMs, these laws are simplified to be functions of only the host subhalo mass and redshift.

¹ In more detailed SAMs, that model e.g. the SF rate as a function of the disk radius (Dutton & van den Bosch 2009; Fu et al. 2010) one needs to assume an ad-hoc density profile within the disk.

2.2.1 Quiescent evolution

Galaxies that do not experience merger events are termed to evolve ‘quiescently’. Each galaxy is modeled by three phases of baryons,

$$\text{a galaxy : } (m_{\text{star}}, m_{\text{cold}}, m_{\text{hot}}). \quad (1)$$

The definitions of m_{cold} and m_{hot} are motivated by the HYD: m_{cold} is the mass of the cold and dense gas that is able to form stars (temperature smaller 10^5 K, density larger than 0.1 cm^{-3}), m_{hot} is all the rest of the gas within the host subhalo, including gas that was previously inside the subhalo but was later ejected. The exact definitions of the different gas phases are given in the next section. We note that there exist various different definitions for cold and hot gas in the literature. Although our definition agrees with the approach adopted by SAMs, it is different from recent studies based on HYDs, as will be discussed below. In addition to our standard model, we will test various scenarios with differing number of gas phases.

In the following we lay out the basic set of differential equations that describe the evolution of these phases using a small set of a priori physical assumptions. These equations have been the basis for the standard paradigm of galaxy formation for over 30 years now (Rees & Ostriker 1977; Silk 1977; White & Rees 1978; White & Frenk 1991).

A fresh supply of gas into the galaxy is provided by smooth accretion along with the growth of the host dark-matter subhalo. The efficiency of hot accreted gas is modeled by

$$[\dot{m}_{\text{hot}}]_{\text{accretion}} = \begin{cases} f_a \cdot \dot{M}_h & \text{if } \dot{M}_h > 0 \\ 0 & \text{otherwise} \end{cases} \quad (2)$$

Here M_h is the subhalo mass, defined as the total mass of dark-matter particles within the subhalo. \dot{M}_h is the growth rate of dark-matter coming from particles that are not included in other subhaloes (not mergers). Square brackets are used to identify individual processes, in this case it is the contribution to \dot{m}_{hot} due to accretion. We allow f_a to be a function of the halo mass and redshift, although in standard SAMs (e.g. Croton et al. 2006) it is a constant that equals the universal baryonic fraction,² $\Omega_b/\Omega_m = 0.1756$. In general, a similar component of cold accretion might exist. However, as will be discussed below, cold accretion is negligible due to our definition of cold gas, which includes a threshold in density.

Hot gas may radiate and cool according to

$$[\dot{m}_{\text{cold}}]_{\text{cooling}} = -[\dot{m}_{\text{hot}}]_{\text{cooling}} = f_c \cdot m_{\text{hot}}. \quad (3)$$

The cooling efficiency, $f_c = f_c(M_h, z)$, is a function of the host halo mass M_h and the redshift only, and is written in units of Gyr^{-1} . We assume that the SF rate is proportional to the amount of cold gas,

$$[\dot{m}_{\text{star}}]_{\text{SF}} = -[\dot{m}_{\text{cold}}]_{\text{SF}} = f_s \cdot m_{\text{cold}}, \quad (4)$$

where $f_s = f_s(M_h, z)$ has units of Gyr^{-1} . Gas can be heated due to SN explosions and move from the cold phase into the hot. In the HYD used here, core collapse SN events follow star formation after a short delay of 30 Myr. Therefore, the feedback should be proportional to the SF rate,

$$[\dot{m}_{\text{hot}}]_{\text{feedback}} = -[\dot{m}_{\text{cold}}]_{\text{feedback}} = f_d [\dot{m}_{\text{star}}]_{\text{SF}} = f_d f_s \cdot m_{\text{cold}}. \quad (5)$$

² For low mass haloes, reionization introduces a filtering mass scale that gives lower baryon fractions (e.g. Somerville 2002).

Similar to the other ingredients, feedback is modeled by a function of the halo mass and redshift $f_d = f_d(M_h, z)$.

All the processes above can be united into a set of differential equations,

$$\begin{aligned} \dot{m}_{\text{star}} &= f_s \cdot m_{\text{cold}} \\ \dot{m}_{\text{cold}} &= -(f_s + f_d f_s) \cdot m_{\text{cold}} + f_c \cdot m_{\text{hot}} \\ \dot{m}_{\text{hot}} &= f_d f_s \cdot m_{\text{cold}} - f_c \cdot m_{\text{hot}} + f_a \cdot \dot{M}_h. \end{aligned} \quad (6)$$

Each physical process is described by one function (f_x), resulting in a set of linear inhomogeneous differential equations. The hot accretion, $f_a \cdot \dot{M}_h$, is the ‘source term’ that governs the total baryonic mass within each galaxy. The other three efficiencies (f_s , f_c , f_d) define the complex evolution of gas and stars within a galaxy.

2.2.2 Satellite galaxies

In this work we assume that each subhalo includes only one galaxy. Since subhaloes might contain only star particles, small subhaloes inside massive FOF groups can survive longer than in dark-matter only simulations. We note that although our SAM uses only the dark-matter mass for each subhalo, the location of the subhalo and its merging time are affected by the dynamical processes within the HYD, including contributions from the gas and star particles. Satellite subhaloes are defined as all subhaloes inside a FOF group except for the central (most massive) subhalo. Because galaxies and subhaloes have a one-to-one correspondence, we use the same terminology for central and satellite galaxies.

While satellite galaxies move within their FOF group, they suffer from mass loss due to tidal stripping. This is modeled by additional terms in the differential equations above:

$$\begin{aligned} \dot{m}_{\text{star}} &= f_s \cdot m_{\text{cold}} \\ \dot{m}_{\text{cold}} &= -(f_s + f_d f_s + \alpha_c) \cdot m_{\text{cold}} + f_c \cdot m_{\text{hot}} \\ \dot{m}_{\text{hot}} &= f_d f_s \cdot m_{\text{cold}} - (f_c + \alpha_h) \cdot m_{\text{hot}} + f_a \cdot \dot{M}_h. \end{aligned} \quad (7)$$

The additional terms including α_h , α_c are computed only for satellite galaxies, and describe the stripping of hot and cold gas respectively. In general, a similar parameter for stellar stripping can be added, but it is negligible in the analysis done here. Our model allows for the stripped mass to be added to the central object, or to be lost to the inter-galactic medium. For satellite galaxies, all the efficiency values f_c , f_d , f_s are based on the subhalo mass at the last time the subhalo was central within its FOF group.

2.2.3 Mergers

In case a subhalo merges into a more massive one, we merge the corresponding galaxies as well, and at the same time. Mergers can trigger SF bursts, with an efficiency that depends on the mass ratio of the two galaxies:

$$\Delta m_{\text{star}} = 0.56(m_2/m_1)^{0.7} \times m_{\text{cold}}, \quad (8)$$

where m_1 , m_2 are the baryonic mass of the central and satellite galaxy respectively, and m_{cold} is the sum of the cold gas masses of the two galaxies. This recipe follows the results of hydrodynamical simulations by Mihos & Hernquist (1994) and Cox et al. (2008), and was adopted by various SAMs (Somerville et al. 2001; Croton et al. 2006; Khochfar & Silk 2009; Neistein & Weinmann 2010). However, as will be explained below, we do not find a strong evidence that these bursts are necessary to reproduce the HYD galaxies, and we therefore do not include bursts in our final implementation of the model.

2.3 How to turn a HYD into a SAM

We would like to extract the effective laws that govern the evolution of galaxies within the HYD. In the language of our SAM, we need to identify the functions f_c, f_s, f_d, f_a that summarize the processes of cooling, SF, feedback, and accretion. For satellite galaxies, we need to determine the constants α_c, α_h that describe the stripping rates of cold and hot gas. In order to do so we follow each subhalo within the HYD along with its merger-tree over time, and keep track of all the particle information. As in the SAM, we assume each subhalo includes exactly one galaxy.

At each snapshot we define three different mass components for each galaxy:

- The stellar mass, m_{star} , defined as the total mass of all star particles within the subhalo.
- The mass of cold gas, m_{cold} , is the mass of all particles that are able to form stars within the subhalo. According to the SF law being used by the HYD, these are all particles with local gas densities larger than 0.1 cm^3 and temperatures lower than 10^5 K .
- The component of hot gas, m_{hot} , includes all gas particles that do not belong to m_{cold} , as well as all particles that were once within the subhalo, but were ejected later. These ejected particles are assigned to the same subhalo only if they did not become part of other subhaloes. Note that usually in SAMs the ejected gas is treated as a different gas component.

We keep track of all particles that belong to subhaloes within the HYD, and check which of them have changed their phase (i.e. $m_{\text{cold}}, m_{\text{star}}, m_{\text{hot}}$) between two subsequent snapshots, or were accreted/stripped. For each galaxy i we define all possible transition rates of the kind $R_{\text{cold} \rightarrow \text{star}}^i, R_{\text{cold} \rightarrow \text{hot}}^i, R_{\text{hot} \rightarrow \text{cold}}^i$, we also checked that other rates, like $R_{\text{hot} \rightarrow \text{star}}^i$ are negligible. For example, in order to compute the SF rate we use the following sum:

$$R_{\text{cold} \rightarrow \text{star}}^i = \frac{1}{\Delta t} \sum_j m_j. \quad (9)$$

Here m_j is the mass of the particle j , and the sum goes over all particles that started as m_{cold} at the beginning of the time-step, and ended as stellar particles. Δt is the time in Gyr between the two snapshots considered. In order to compute cooling (or heating) rates we use a similar sum, taking into account all particles that started as hot (cold) particles at the beginning of the time-step, and ended as cold (hot).³

For the accretion rate, $R_{\text{hot} \rightarrow \text{hot}}$, we use the sum over all particles that joined the hot component of the subhalo, and were not identified inside other subhaloes before. In addition, we take into account the mass of particles that were exchanged between subhaloes that belong to different FOF groups. This means that particles that are stripped into a different FOF group are subtracted from the accretion rate. On the other hand, particles that join the central subhalo coming from satellite subhaloes within the same FOF group are not accounted for in accretion rates.

Whenever we have a merger event, we first sum up the components of the progenitor galaxies, and only then compute the rates

³ Multiple transitions of the type hot \rightarrow cold \rightarrow hot might exist between two snapshots, but these are negligible according to the cooling time-scales that will be shown below. In case multiple transitions exist, not including them will modify the rates we measure. However, these modifications should not change the mass components of the SAM galaxies. This issue reflects the inherent degeneracy of the model equations.

for the remnant galaxy. This means that our rates reflect the quiescent evolution only, and do not include mergers explicitly. However, mergers might still induce bursts both in the HYD and SAM, following, e.g., Eq. 8. Mergers can also affect other processes indirectly, like heating, cooling or SF within the HYD. This issue will be discussed below.

The efficiencies for each galaxy i are defined by normalizing the rates:

$$f_a^i = \frac{R_{\text{hot} \rightarrow \text{hot}}^i}{\dot{M}_h^i}, \quad (10)$$

$$f_c^i = \frac{R_{\text{hot} \rightarrow \text{cold}}^i}{m_{\text{hot}}^i}, \quad (11)$$

$$f_s^i = \frac{R_{\text{cold} \rightarrow \text{stars}}^i}{m_{\text{cold}}^i}, \quad (12)$$

$$f_d^i = \frac{R_{\text{cold} \rightarrow \text{hot}}^i}{R_{\text{cold} \rightarrow \text{stars}}^i}. \quad (13)$$

In order to obtain the global efficiency law, for the full cosmological box, we consider only central subhaloes within their FOF groups. We then split the sample of subhaloes into bins of different mass and redshift. For each bin the average efficiency is defined by averaging the nominator and denominator separately. For example,

$$f_s(M_h, z) \equiv \frac{\langle R_{\text{cold} \rightarrow \text{star}}^i \rangle}{\langle m_{\text{cold}}^i \rangle}. \quad (14)$$

Here averaging is done over all galaxies within the same M_h and z bin. Quite arbitrarily, we choose bins of 0.2 dex in M_h , and 7 bins in cosmic time, spaced by ~ 2 Gyr. We have checked that finer bins do not modify the results of this work.⁴ The bins in cosmic time are much wider than the time between two subsequent snapshots. Consequently, the time average typically includes 10 different snapshots.

When computing the accretion efficiency, we use the fact that within the SAM, negative dark-matter accretion events are treated as zero, and are not inducing negative gas accretion. To make this approach consistent with the average value of f_a measured from the HYD, we set all negative values of \dot{M}_h to zero first, only then do we average \dot{M}_h and compute f_a :

$$f_a(M_h, z) \equiv \frac{\langle R_{\text{hot} \rightarrow \text{hot}}^i \rangle}{\langle \max(\dot{M}_h, 0) \rangle}. \quad (15)$$

This way of averaging guarantees that the total baryonic mass within our SAM galaxies will agree with the HYD.

We have saved stripping and accretion rates for satellite galaxies, and recorded the amount of mass flowing into the central subhalo, in comparison to the total mass being stripped. In general, the stripped mass is best described by a normalized efficiency, i.e. the ratio $\alpha_h = \Delta m_{\text{hot}}/m_{\text{hot}}$, as was defined in Eq. 7. However, we found that both α_h and α_c are changing as a function of the host subhalo mass and redshift. In addition, the efficiencies of feedback and cooling for satellite galaxies are somewhat different than those for central galaxies. This partially depends on the definitions of the various gas phases, and how each is being stripped. In this work we have chosen the simplest model possible, taking into account only constants α_c and α_h . Furthermore, we use the same cooling and feedback efficiencies as for central galaxies. We will show below

⁴ The SAM used here (Neistein & Weinmann 2010) automatically interpolates the input values of f_s, f_a, f_c, f_d into a fine grid in halo mass and time.

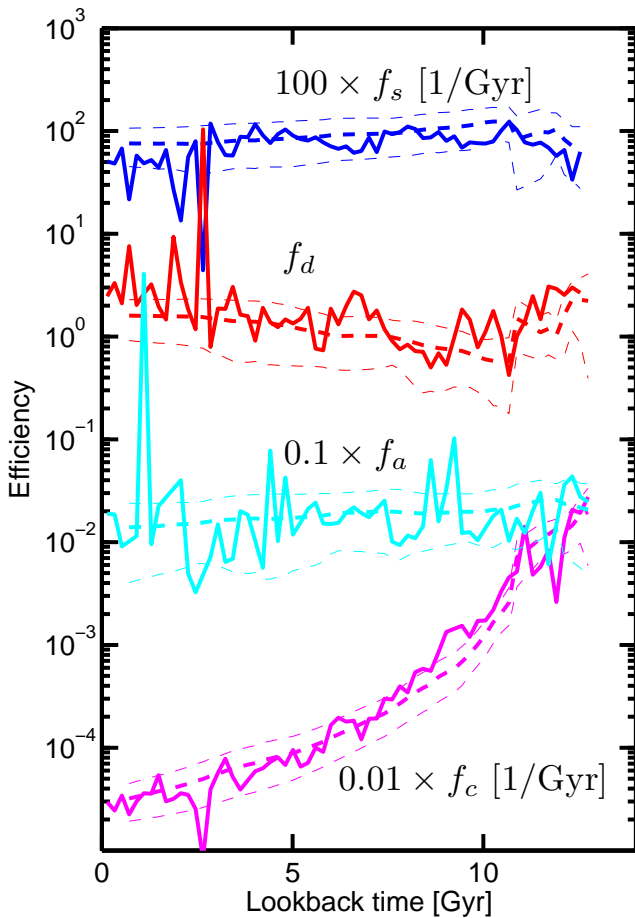


Figure 1. The efficiencies of cooling, accretion, SF, and feedback following the main-progenitor history of a specific galaxy within the HYD, hosted by a subhalo of mass $\sim 10^{14} M_{\odot}$ at $z = 0$. *Solid lines* show the different efficiencies for this galaxy as measured from the HYD at all snapshots. The *thick dashed lines* correspond to the average efficiency for all galaxies within the HYD, including only central galaxies with the same host subhalo mass and at the same redshift as the galaxy plotted in solid lines. The *thin dashed lines* show the standard deviation for the same sample of galaxies above. The mass components of this galaxy are shown in Fig. 2.

that this solution is reasonably accurate for satellite galaxies. We plan to investigate this issue more closely in a future work.

In the hydrodynamical simulation, star particles can lose some of their mass due to stellar winds and SN. This mass loss is computed using a stellar population synthesis model and is added to the surrounding particles (see Wiersma et al. 2009). Although this process can be easily modeled within the SAM, it complicates the interpretation of the results. This is mainly because the stellar mass loss at a given epoch is the outcome of the SF history over a few Gyr. Therefore, the rates measured from the HYD would not be instantaneous, and might include less scatter with respect to the SAM. We therefore assume that all particles have a fixed mass, and compute all rates and efficiencies using this assumption. This assumption is also being used when comparing the results of the HYD against the SAM. Consequently, the total baryonic mass within galaxies is sometimes higher than the universal baryonic fraction.

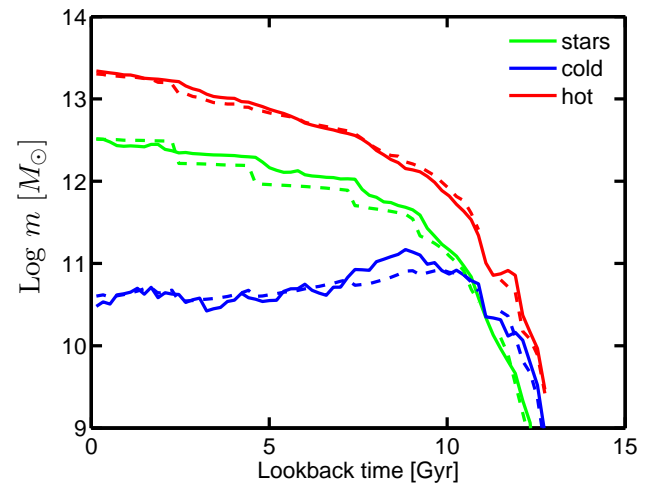


Figure 2. The baryonic components for the main-progenitor history of a specific galaxy. *Solid lines* show the mass of stars, cold gas, and hot gas as measured from the HYD. *Dashed lines* represent the same components within our SAM, using the same dark-matter subhaloes (see section 4). The efficiencies of cooling, accretion, SF, and feedback for the same galaxy are plotted in Fig. 1.

For completeness, we show in the Appendix all the efficiencies from the HYD when using the proper mass for each particle, as was used in the simulation.

In Fig. 1 we show the different efficiencies for the main-progenitor history⁵ of one massive galaxy within the HYD, in comparison to the global averages using all central subhaloes of the same mass and time within the HYD. It seems that the randomness in the efficiencies of one galaxy is not too big, and is averaged out over time (except for a few narrow peaks that should not affect the masses of stars and gas significantly). For example, f_c and f_a show deviations on time-scales of one snapshot (200 Myr), with no significant trends over larger time-scales. On the other hand, f_d and f_s show deviations from the average efficiencies that are lasting for ~ 2 Gyr. Overall, the behaviour of one galaxy seems to be very regular, and does not show significant deviations larger than the standard deviation (STD) computed using all the galaxies in the HYD. The total mass in stars, cold gas, and hot gas for the same galaxy are plotted in Fig. 2. We will show below that once we use the SAM over the same merger-trees, the agreement between HYD and SAM is very good, also when comparing individual objects.

3 THE PHYSICS OF THE HYD

The different efficiencies extracted from the HYD should describe the various physical processes involved in forming galaxies. As we will see below, they allow the SAM to accurately reproduce the population of galaxies in the HYD. This means that we have a reliable estimate of the net effect that heating, cooling, accretion, and SF have on galaxies within the HYD.

⁵ The main-progenitor history is defined by following back in time the most massive progenitor in each merger event. Note that at high redshift, the subhalo that belongs to the main-progenitor branch might not be the most massive within its merger tree.

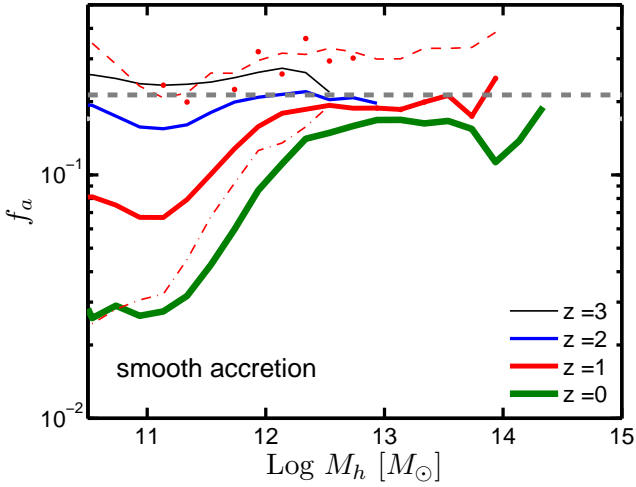


Figure 3. The smooth accretion rate of baryons as derived from the hydrodynamical simulation. f_a is defined as the ratio of the smoothed hot accretion, over the dark-matter smooth accretion, averaged in bins of halo mass and time. Each *solid line* represents a different redshift bin, all the other lines are shown only for $z = 1$: The *dashed line* shows the average plus one standard deviation in f_a ; The *dotted-dashed line* shows the average minus one standard deviation, after averaging out f_a for all the progenitors within each tree, and at ~ 10 different snapshots (all the merger-trees are rooted at $z = 0$); The *dots* represent the average plus one standard deviation of f_a after averaging over different progenitors within a tree, but not within different snapshots. The thick dashed line is the universal baryonic fraction, $\Omega_b/(\Omega_m - \Omega_b) = 0.213$.

3.1 Smooth accretion

The values of the accretion rate, f_a , that were extracted from the HYD are shown in Fig. 3. We plot only the ‘hot accretion’ component as we do not detect an accretion of cold gas into galaxies. Although this seems to be in conflict with various recent studies (e.g. Kereš et al. 2005, 2009; Dekel et al. 2009; van de Voort et al. 2011) it is a result of the different definitions of ‘cold gas’ that are being used in the literature. Here we define cold gas as the gas that is able to form stars, requiring high densities (larger than 0.1 cm^{-3}), and not only low temperatures. This is a different definition from most other studies based on HYDs, that often define a gas particle to be cold if it was not previously heated to the virial temperature of its halo. Here we adopt a more straight-forward definition of cold gas, based on the SF law. Using our definition, there is no evidence for ‘cold accretion’ at all redshifts and for all subhalo masses. This fact is reasonable, because star-forming gas might form stars before it joins the subhalo, and will therefore be identified as a separate galaxy.

Unlike in standard SAMs, where f_a is assumed to be a constant, here f_a shows a significant dependence on the subhalo mass, decreasing by a factor of ~ 10 from subhalo masses of 10^{13} to $10^{11} M_\odot$ at $z = 0$. This is surprising, considering the fact that all galaxies used here are the central objects inside their FOF groups. We have checked this effect further, and tested a model in which negative gas accretion (stripping) is allowed whenever the dark-matter mass decreases. Using this new assumption, the accretion efficiencies become much closer to a constant, with deviations of a factor of ~ 2 , consistent with van de Voort et al. (2011) (the equivalent plot of f_a in this case is shown in the Appendix, Fig. A1). Our conclusion is that the low accretion rates shown here for low-mass

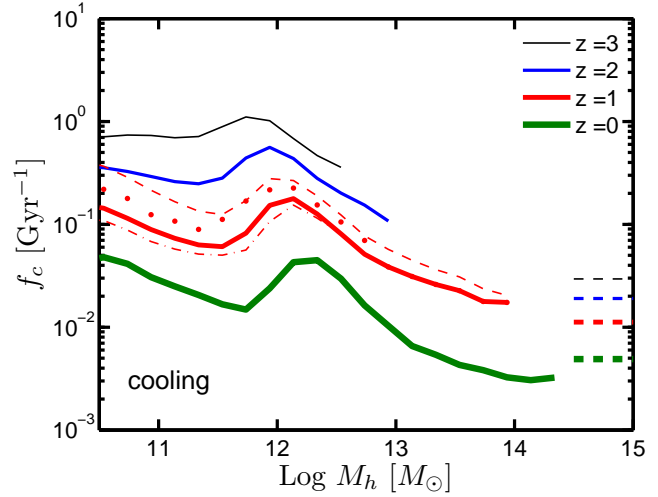


Figure 4. The cooling efficiencies extracted from the HYD, and averaged as a function of halo mass and time. f_c is defined as the ratio of the cooling rate over the mass of hot gas. Plotted lines are using the same definitions as in Fig.3. *Dashed lines* on the bottom right are proportional to one over the cosmic time.

subhaloes are compensating for the negative accretion events. Models based on *average* dark-matter accretion rates should therefore use the efficiencies quoted in the Appendix. We have also checked that the total baryonic fraction within galaxies agrees with the accretion rates given in the Appendix. In terms of the comparison made here, once we include a mechanism for gas stripping within central galaxies, following the dark-matter evolution, we do not get a better agreement between the HYD and SAM. We therefore adopt the solution of positive accretion only, as it is more simple to implement.

As was discussed in section 2.3, the accretion rates shown here are based on a fixed particle mass, without taking into account the mass loss due to stellar winds and SN within the HYD. Consequently, accretion rates can have values larger than the equivalent cosmic value, $\Omega_b/(\Omega_m - \Omega_b)$. In the Appendix we plot all the efficiencies using the proper mass for each particle within the HYD. This effect changes the overall normalization of each efficiency slightly, but it does not change the trends with subhalo mass and time.

3.2 Cooling

The next process for which the efficiencies are required is cooling. In Fig. 4 we show average cooling efficiencies for all the galaxies within the HYD. Here we should keep in mind that the component of ‘hot gas’ includes gas particles that were ejected out of the subhalo. Therefore, the cooling efficiencies are normalized by the sum of both ejected and hot gas, according to Eq. 11. For a different definition of cooling efficiencies, where hot and ejected phases are treated separately, we refer the reader to the Appendix. We note that the dip in the cooling efficiencies seen at a subhalo mass of $\sim 7 \times 10^{11} M_\odot$ is due to the combination of both hot and ejected phases.

In general, cooling efficiencies are showing a roughly constant behaviour as a function of subhalo masses for subhaloes lower than $\sim 10^{12} M_\odot$, and go down for more massive subhaloes. This is qualitatively in agreement with semi-analytic models. However, the

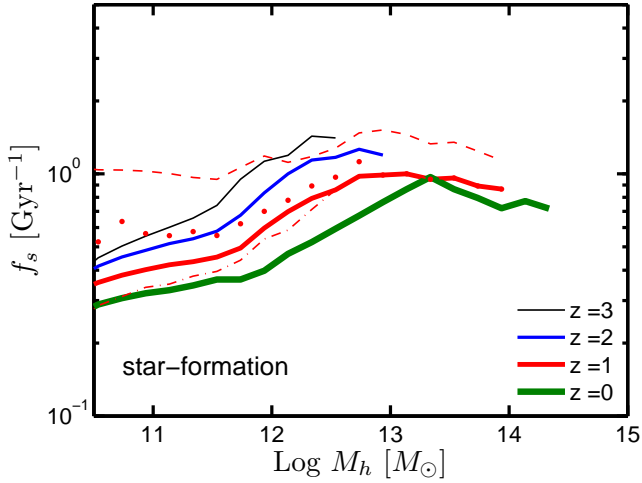


Figure 5. Star-formation efficiencies within the HYD, defined as the ratio of the SF rate over the mass of cold gas. For the line definitions see Fig. 3.

dependence of the cooling efficiencies on cosmic time is stronger than a simple linear dependence. Since the dynamical time within subhaloes is proportional to the cosmic time, cooling cannot be modeled only by the infall time of gas into the centre of haloes. This might be a result of the cooling process itself, and its dependence on the hot gas properties (e.g. McCarthy et al. 2008; Wiersma et al. 2009).

In the terminology of ‘cold accretion’ mode, where all the accreted gas is assumed to be falling in narrow streams (e.g. Dekel et al. 2009), the process of ‘cooling’ describes the time it takes the stream to reach the central disk, and become dense enough to be a part of our definition of m_{cold} . A stronger dependence of cooling on the cosmic time might mean that accretion through filaments is more relevant at high redshift (van de Voort et al. 2011). A different option is that trajectories of streams are more radial at high-redshift. This last fact was already pointed out by Weinmann et al. (2011), and is in agreement with the orbits of subhaloes within cosmological dark-matter simulations (Wetzel 2011; Hopkins et al. 2010).

The cooling efficiencies shown here can be compared to standard SAM algorithms, which are usually following the spirit of White & Frenk (1991). This issue was investigated by various studies in the past (Benson et al. 2001; Yoshida et al. 2002; Helly et al. 2003; Cattaneo et al. 2007; De Lucia et al. 2010; Crain et al. 2010; Lu et al. 2011), mostly claiming some agreement between different SAMs and HYDs, and some noticeable deviations (especially at high redshift). For example, Crain et al. (2010) showed that the algorithm of White & Frenk (1991) strongly overpredict cooling rates due to the specific entropy profiles of gas within haloes. In addition, various SAMs that are based on White & Frenk (1991) can show significant deviations in cooling rates due to the detailed implementation of the algorithm (De Lucia et al. 2010).

We find significant differences when comparing the cooling efficiencies here against the one used by De Lucia & Blaizot (2007) and summarized in Neistein & Weinmann (2010). For example, at $z = 1$, De Lucia & Blaizot (2007) predict cooling efficiency of $\sim 1 \text{ Gyr}^{-1}$ at subhalo mass of $10^{11} M_{\odot}$, roughly a factor of 10 higher than what is found here.

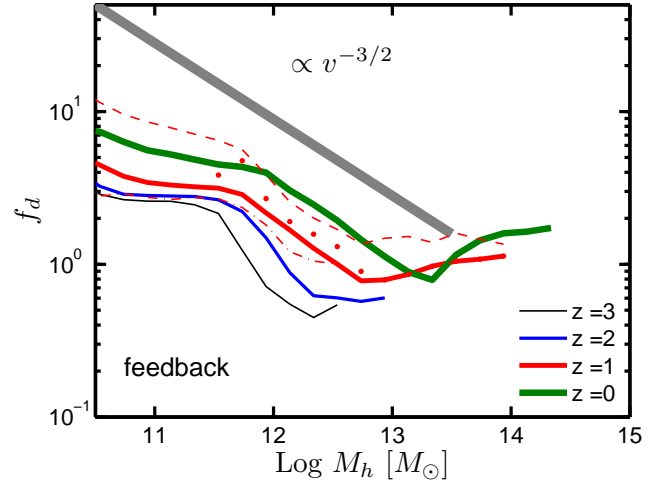


Figure 6. Feedback efficiencies measured from the HYD, and averaged as a function of halo mass and time. f_d is the ratio between the heating rate and the SF rate. The thick gray line is proportional to the virial velocity of subhaloes to the power of $-3/2$, other lines are defined as in Fig. 3.

3.3 Star formation

Fig. 5 shows the SF efficiencies found within the HYD. The time-scales for converting the cold gas into stars range from $\sim 3 \text{ Gyr}$ for low mass subhaloes at $z = 0$, to $\sim 1 \text{ Gyr}$ for massive subhaloes at $z = 3$. The low-redshift values are roughly consistent with the observational constraints (Schiminovich et al. 2010; Saintonge et al. 2011). However, the dependence on redshift found here is much smaller than what is usually assumed in SAMs, where the conversion efficiency is proportional to the cosmic time (see, however, Khochfar & Silk 2009). For example, Wang et al. (2011) showed the SF efficiencies as a function of subhalo mass for various models, where in standard SAMs the difference between $z = 3$ and $z = 0$ reaches an order of magnitude.

Interestingly, the SF efficiencies show a double power-law behaviour as a function of subhalo mass, where the peak efficiency is located at $\sim 10^{12} - 10^{13} M_{\odot}$, depending on the specific redshift. For high-mass subhaloes the SF is not significantly reduced. Consequently, the high fraction of passive galaxies within massive subhaloes is not related to a reduced SF efficiency, but rather to gas consumption, environmental effects (Khochfar & Ostriker 2008), or AGN feedback (e.g. Croton et al. 2006).

3.4 Feedback

The feedback efficiencies extracted from the HYD are plotted in Fig. 6. These seem to follow a power-law of the type $v^{-3/2}$ below subhalo mass of $\sim 10^{13} M_{\odot}$, where v is the virial velocity of the subhalo. Above this mass, the feedback efficiency shows a modest upturn. The feedback efficiency represents gas that is heated from the cold phase into the hot component, and possibly ejected out of the subhalo. Within the OWLS reference model, SN feedback is implemented in kinetic form using a constant wind velocity of 600 km s^{-1} . This causes the feedback to become inefficient for halo masses greater than a few times $10^{11} M_{\odot}$ (Dalla Vecchia & Schaye 2008; Crain et al. 2009; Schaye et al. 2010; Haas 2010).

SAMs usually assume a power-law efficiency with very different indexes. For example, De Lucia & Blaizot (2007) assumed a constant; Cole et al. (2000) have used a power of -2 , following the

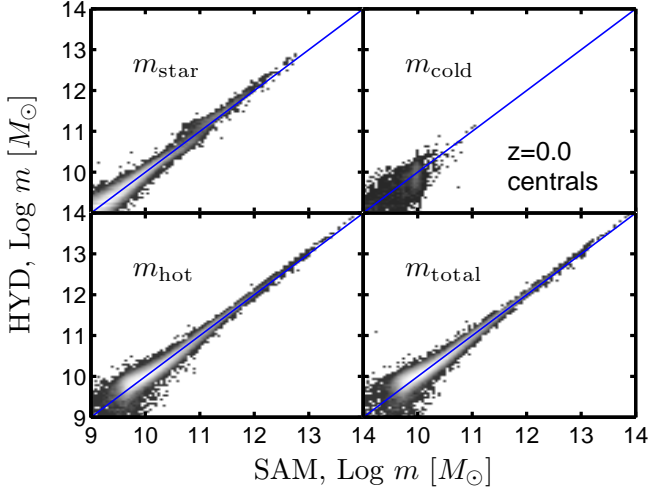


Figure 7. Comparing the masses of individual galaxies, SAM against the HYD. Each panel represents a different mass component as labeled, using only central subhaloes at $z = 0$. The panels show the two dimensional histogram of the pairs $(m_{\text{SAM}}, m_{\text{HYD}})$, describing the mass of the same objects in both models. The pixels are color-coded according to the log of the number of objects. The mean difference between HYD and SAM is lower than 0.08 dex for all mass components. STDs are 0.08 for m_{star} (except for $\sim 10^{11} M_{\odot}$, for which the STD goes to 0.13 dex). For m_{hot} and m_{total} the STD starts at ~ 0.08 dex for low mass galaxies and reaches ~ 0.04 for massive galaxies. The STD for m_{cold} is around 0.2 dex.

potential of the host halo; and Guo et al. (2011) assumed a power of -3.5. All these are very different from what is found here. The feedback efficiency within a model that includes three phases of gas (m_{cold} , m_{hot} , and m_{ejc}) is plotted in the Appendix.

4 COMPARING MODEL GALAXIES

In this section we compare the results of the SAM with the HYD. The SAM uses only the physical ingredients that were described above, i.e., f_a , f_c , f_s and f_d , and was run using merger-trees extracted from the same HYD. We specifically use the same values plotted in Figs. 3–6, using three more bins in cosmic time. As was explained in section 2.3, in order to keep the model simple we do not attempt to model satellite galaxies with full accuracy. We set the values of α_c and α_h to 0 and 0.3 respectively, because they provide an effective behaviour which is similar to that of the HYD. The stripped gas is added to the central galaxy within the FOF group. Other than that, the SAM has no free parameters, and no tuning was done.

The model galaxies from the HYD and our SAM are compared in Fig. 7. By matching the same subhaloes from the HYD & SAM, we are able to show the agreement between the models on an object-by-object basis. Unlike in previous studies that showed large deviations between SAM and HYD galaxies (e.g. Hirschmann et al. 2011), here the two models agree quite well. For central galaxies the STD of differences is less than 0.1 dex, for all redshifts and for the various galaxy components (except for m_{cold} , which usually includes only a few tens of particles within a galaxy). The total mass in baryons, $m_{\text{total}} \equiv m_{\text{star}} + m_{\text{cold}} + m_{\text{hot}}$, is shown as a probe of the accuracy of the accretion rates, f_a . Note that the mass of gas particles within the simulation is $8.64 \times 10^7 h^{-1} M_{\odot}$, so

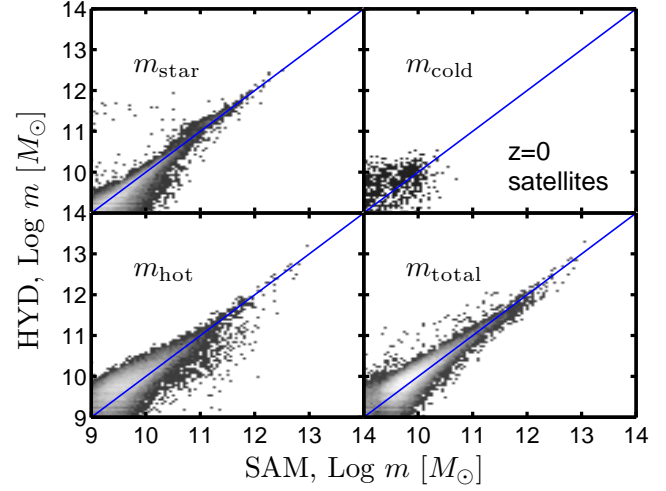


Figure 8. Comparing the mass of individual galaxies, SAM against the HYD. Data was derived in the same way as in Fig. 7, but for the population of satellite galaxies at $z = 0$. Mean (STD) differences between SAM and HYD reach 0.1 (0.2) dex for both m_{star} and m_{total} , and 0.3 (0.5) dex for m_{hot} .

masses below $10^{10} M_{\odot}$ include less than 100 particles and suffer from various numerical artifacts, also within the HYD.

We found that deviations between m_{total} in the SAM and the HYD correlate strongly with deviations in m_{hot} , and are the reason for most of the scatter found in m_{hot} . This is a consequence of the fact that most of the baryonic mass is located in m_{hot} . A similar (but weaker) correlation exists between deviations in m_{total} and m_{star} . Even though the stellar mass is affected from various additional processes that seem to be more complicated than accretion, the deviations in f_a between the HYD and the SAM still affect m_{star} . This fact can also be seen in Figs. 3–6. In these plots we show the STD of each efficiency at $z = 1$, after averaging out all progenitors of the same galaxy at $z = 0$ (dotted-dashed lines). It is evident that the scatter in f_a between different galaxies is significantly higher than the scatter in other efficiencies. This might be a result of different merger-histories for subhaloes that live inside different environment densities (the assembly bias effect, Gao et al. 2005).

The small scatter in m_{star} between the HYD and the SAM (0.08 dex) is interesting in view of the larger scatter in m_{cold} (0.2 dex). Although the masses of m_{cold} are usually below $10^{10} M_{\odot}$, and are therefore not numerically reliable, these masses are responsible for making stars, and somehow produce a small scatter in m_{star} . This issue will be discussed in section 6.3. A different contribution to the scatter in m_{cold} comes from mergers, and will be discussed in section 4.1.

We have explored the larger scatter in m_{star} at values of 10^{11} by running a different HYD, with a different feedback model (Dalla Vecchia & Schaye, in preparation), and by increasing the resolution of the efficiency bins (both in mass and time). The high-resolution efficiencies were not making any noticeable change, but the HYD with a different feedback model results in a significant smaller scatter at $m_{\text{star}} = 10^{11} M_{\odot}$. It might be that the kinetic feedback prescription used by the HYD affects the hydrodynamical state of the gas in a way that is different than other cooling and heating channels. These changes might complicate the simple distinction done here between cold and hot gas. In addition, it might be that the

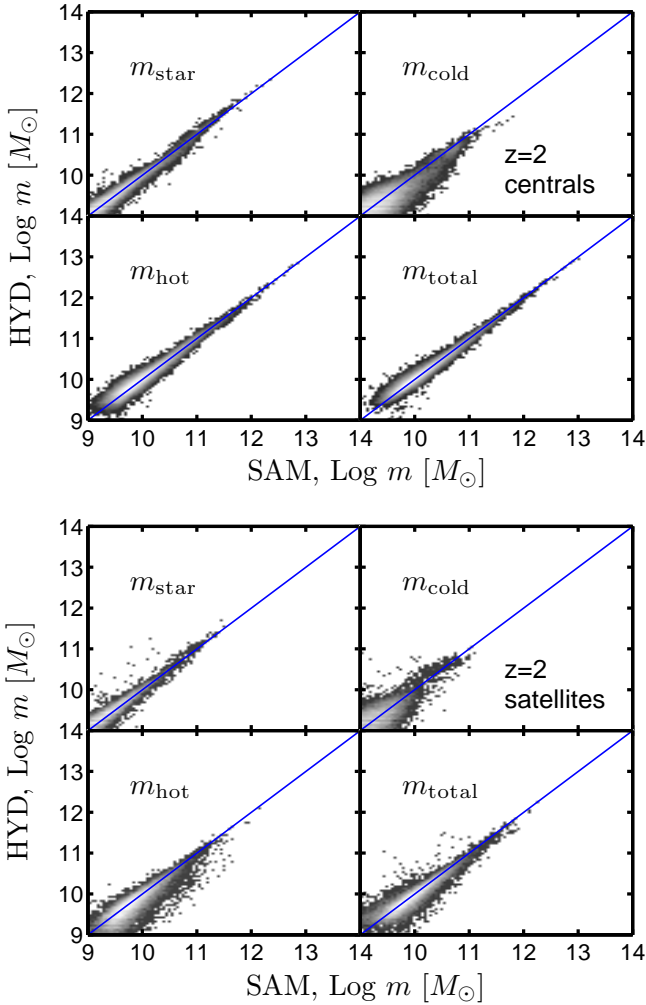


Figure 9. Comparing the mass of individual galaxies, SAM against the HYD. Histograms are the same as in Fig. 7, but for the population of central and satellite galaxies at $z = 2$. For central galaxies, the mean and STD of differences between HYD & SAM are similar to the numbers quoted in Fig. 7. For satellite galaxies the agreement is roughly two times better than in Fig. 8 (in dex units).

transition between effective and ineffective feedback is sensitive to other properties of the subhaloes other than the subhalo mass.

A comparison for satellite galaxies at $z = 0$ is shown in Fig. 8. Here the deviations between the SAM and the HYD are larger than for central galaxies, reaching 0.2 dex for m_{star} . We have tried a model in which stripping of satellite galaxies follows the stripping of dark-matter, according to Weinmann et al. (2010). This model did not improve the match between the HYD and the SAM, probably because satellite galaxies experience on average different efficiencies of cooling and feedback, as was discussed in section 2.3. This can be seen in Fig. 8, where m_{total} for satellite galaxies behaves better than m_{star} and m_{hot} , hinting that the total amount of stripping is modeled properly. The physics of satellite galaxies is complicated, and deserves more attention than we give it in this work.

In Fig. 9 we compare galaxies at $z = 2$, finding similar trends to $z = 0$ as discussed above. The mass of cold gas is much higher at this redshift, so the agreement and deviations are clearer. For satellite galaxies the agreement is much better than at $z = 0$, probably

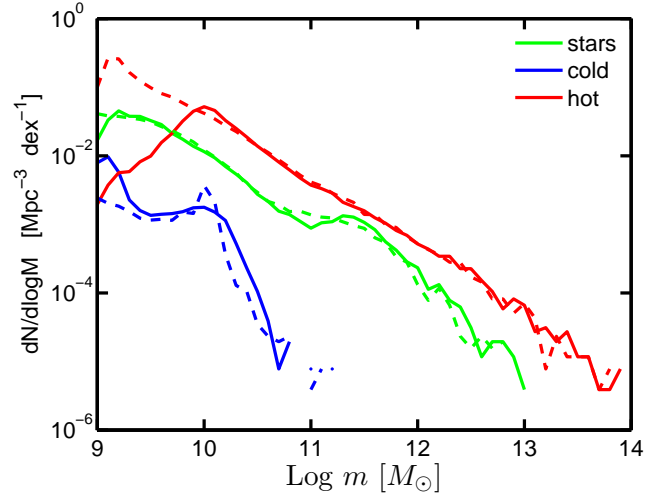


Figure 10. The mass functions of m_{star} , m_{cold} , and m_{hot} in the HYD (solid lines) and in the SAM (dashed lines). All galaxies at $z = 0$ are selected.

because these galaxies had much less time to evolve within their group, and deviations have not accumulated yet.

The mass functions for m_{star} , m_{cold} , and m_{hot} using both the HYD and the SAM are shown in Fig. 10. Overall, the agreement between the two models is very good for all mass components. This is expected, as the agreement for individual objects is good. For $m_{\text{hot}} < 10^{10} M_{\odot}$ the sensitivity of the HYD to resolution effects seems to be high. This probably hints to the dependence of the cooling mechanisms on resolution. Fig. 10 includes all the galaxies within each model. We note that the other figures in this section only show galaxies that exist *both* in the SAM and in the HYD. Due to our definitions, galaxies that just emerged within the HYD (and do not have any progenitors) are not included in the SAM. On the other hand, the SAM keeps a small population of galaxies that do not have descendant subhaloes. These two populations are quite small and do not affect the mass functions.

The SF rates for individual objects are compared in Fig. 11. Unlike the integrated properties shown above, the SF rates show stronger deviations between the two models, with a STD of ~ 0.5 dex. The scatter in m_{cold} is about 0.2 dex, meaning that the deviations in the SF rate are dominated by variations in the SF efficiency. In addition, most of the population of galaxies at low redshift form stars at a low rate, $\sim 1 M_{\odot} \text{ yr}^{-1}$. This rate corresponds to just a few gas particles within a snapshot, increasing the scatter between HYDs and SAMs. As can also be seen in Fig. 5, the scatter in f_{s} between all galaxies is large, reaching a factor of 3 for low mass subhaloes. However, when f_{s} is averaged over all the progenitors within a tree, and over a few snapshots, the scatter goes down dramatically. Apparently, the deviations in SF rates result in much smaller deviations for stellar masses. We will examine this issue in section 6.3.

4.1 How important are merger-induced bursts?

Our SAM does not include any merger-induced processes, like SF bursts, heating or cooling. We have tested the contribution of mergers to the models in various ways. First, we have computed the average baryonic efficiencies after excluding galaxies that had a major merger event in the last 0.5 Gyr, or that have a major satellite

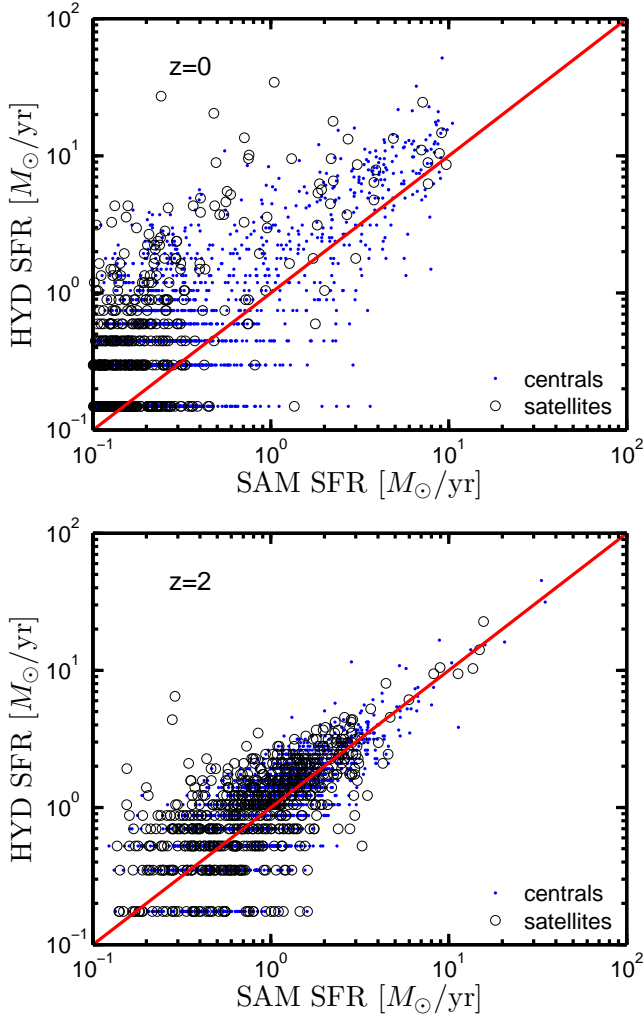


Figure 11. Comparison of SF rates for individual galaxies within the models, SAM against the HYD. Central and satellite subhaloes are plotted in dots and circles respectively. The solid line shows the values where both SF rates agree. Top and bottom panels show results for $z = 0$ and $z = 2$, respectively.

galaxy at a distance smaller than 0.5 Mpc (‘major mergers’, and ‘major satellite’ are defined to have a mass ratio larger than 0.2). Applying this selection criterion does not change the results of the efficiencies in a noticeable way. The agreement between the SAM and HYD galaxies does not change either. There is only a minor change in the average agreement in m_{total} . However, it might be that the *number* of merger events is small, and cannot affect the full population of galaxies within a cosmological box.

A second test we carried out is to run our SAM with an additional recipe for merger-induced SF bursts. We have used the standard recipe given in Eq. 8 above. However, in terms of the comparison made here, this recipe does not change the agreement between the HYD and the SAM.

Since the effect of mergers might accumulate with time, we would like to define a quantity that is related to the number of mergers a galaxy had in its past. Consider a galaxy at $z = 0$, and define the mass in stars, m_i ($i > 1$), that was accreted from each satellite galaxy i within the merger tree. All the stars that were formed within the main-progenitor branch are termed m_0 . Using m_{star} , the stellar mass of the galaxy today, we define:

$$\sigma_m = \sqrt{\sum_{i \geq 0} \left(\frac{m_i}{m_{\text{star}}} \right)^2}. \quad (16)$$

If the stellar mass of a galaxy is built from N_s equal values of m_i , then σ_m would equal $1/\sqrt{N_s}$. Low values of σ_m indicate on many merger events, while high values (close to unity) indicate that the galaxy is built from one branch only. The meaning of using σ_m can be related to the comparison we make between the HYD and the SAM. Assume that each progenitor galaxy within the SAM includes some random, normally distributed error in stellar mass (with respect to the HYD), that is proportional to its mass, m_i . In this case the relative error in the sum of all masses (i.e. the error in the SAM prediction for m_{star}) will equal σ_m .

We have computed σ_m for each galaxy within our SAM, and measured the correlation between σ_m and the deviations between the SAM and HYD galaxies. We found that the mass within the SAM galaxies is higher than within the HYD for galaxies with more mergers (galaxies with lower σ_m). This effect is true for all mass components (m_{star} , m_{cold} , and m_{hot}), but it is strongest for m_{cold} . This means that galaxies within the HYD lose some of their mass in each merger event, or that satellite galaxies lose some of the stripped mass to the inter-galactic medium. This effect is not modeled by our current SAM, but it should be straight forward to add it, once the treatment of satellite galaxies is more accurate.

To conclude, we do not find any significant evidence for merger-induced SF bursts within the HYD used here. This seems to be in conflict with previous simulations of galaxy mergers (e.g. Mihos & Hernquist 1994; Cox et al. 2008). However, as was suggested by Moster et al. (2011), it might be that the presence of hot gas in subhaloes regulates the efficiency of bursts within our simulation. It might also be that the mass gained in bursts does not contribute much to the total stellar mass within galaxies (Khochfar & Silk 2006), and that mergers are too rare (Lotz et al. 2008; Hopkins et al. 2010). On the other hand, we do find significant evidence for mass loss within mergers, as was pointed out by previous studies (Monaco et al. 2006; Purcell et al. 2007; Conroy et al. 2007; Yang et al. 2009).

5 THE ONE-PHASE MODEL

The analysis above was based on a SAM with two different gas phases within a galaxy, m_{cold} and m_{hot} . As an alternative, this section describes a model with only one phase of gas, allowing us to study the uniqueness of the SAM equations. The one-phase model has been explored by other studies in the past. In one of the earliest SAM works, Cole (1991) used modelling of cold gas in haloes to predict the galaxy luminosity function. Although SAMs are usually based on three phases of gas in galaxies, the one-phase model was recently explored by Bouché et al. (2010); Krumholz & Dekel (2011); Khochfar & Silk (2011); Davé et al. (2011). In what follows, we will try to emphasize the points of similarity and difference with respect to these previous works.

5.1 A SAM with one phase of gas

For each galaxy we define

$$m_{\text{gas}} = m_{\text{hot}} + m_{\text{cold}}. \quad (17)$$

Thus, m_{gas} includes all gas particles within the subhalo, as well as gas particles that were ejected from the halo. In this case, the

equations that govern galaxy evolution are:

$$\begin{aligned}\dot{m}_{\text{star}} &= \tilde{f}_s \cdot m_{\text{gas}} \\ \dot{m}_{\text{gas}} &= -\tilde{f}_s \cdot m_{\text{gas}} + f_a \cdot \dot{M}_h.\end{aligned}\quad (18)$$

Within the SAM, these equations assume that \tilde{f}_s and f_a are independent of the galaxy components m_{star} and m_{gas} . However, if we compare this model to the standard model with the two phases above (Eq. 6), we get that $\tilde{f}_s = f_s m_{\text{cold}}/m_{\text{gas}}$. Consequently, if the standard model is accurate, the one-phase model cannot be treated as a set of ordinary differential equations as we assume below.

The one phase model is useful because it is simple, and in case \tilde{f}_s does not depend on m_{gas} , it can be integrated to follow the evolution of one object, with no mergers. First, we define the integral,

$$P(t_0, t_1) = \exp \left[- \int_{t_0}^{t_1} \tilde{f}_s dt \right], \quad (19)$$

where the values of \tilde{f}_s within the integrand are computed for the specific mass history of the subhalo. Once P is computed, the solution of the set of equations can then be written as

$$\begin{aligned}m_{\text{gas}}(t) &= m_{\text{gas}}(t_0) P(t_0, t) + \\ &P(t_0, t) \int_{t_0}^t \frac{f_a(t_1) \dot{M}_h(t_1)}{P(t_0, t_1)} dt_1\end{aligned}\quad (20)$$

It should be emphasized that this solution is valid for one branch only, and cannot be expanded easily to include all the progenitors within a merger-tree. This is because both f_a and \tilde{f}_s depend on the mass of each progenitor.

A model with one gas phase can be written in various ways. For example, we could have a model that is based only on the cold gas within a galaxy, as was done by Bouché et al. (2010); Khochfar & Silk (2011) and Davé et al. (2011). It is evident from Eqs. 6 that a straightforward way to do it is to assume that the hot gas component equals the *total* baryonic mass, neglecting the 3rd equation, and keeping the two first equations almost unchanged. It should be noted that we then get a set of equations that is different from the above studies. Here the source term is not $f_a \dot{M}_h$, but $f_c \tilde{f}_a \dot{M}_h$, where \tilde{f}_a represent the fraction of hot gas within the subhalo. Since this approach is different from our standard model, we do not explore it further here.

We have also tested a model that includes three phases of gas, using m_{ejc} in addition to the two phases in the standard model. The mass within m_{ejc} takes into account all the gas particles that were ejected from the subhalo. These are part of m_{hot} in the standard two-phase model. For most of the results quoted below, this model shows a similar agreement to the HYD, and is thus not discussed in detail. We present the feedback and cooling efficiencies computed for this model in the Appendix.

5.2 Star formation

In Fig. 12 we plot SF efficiencies for the one-phase model, describing the efficiency of transforming the total amount of gas within a subhalo into stars. The values of \tilde{f}_s combine the behaviour of f_s , f_c , and f_d from the standard model into a one, compact form (see Eq. 18).

The values of \tilde{f}_s shown in Fig. 12 are different from what is usually assumed within one-phase models (Bouché et al. 2010; Krumholz & Dekel 2011; Khochfar & Silk 2011; Davé et al. 2011). For example, the SF efficiency derived from our HYD changes rapidly as a function of subhalo mass, while other works

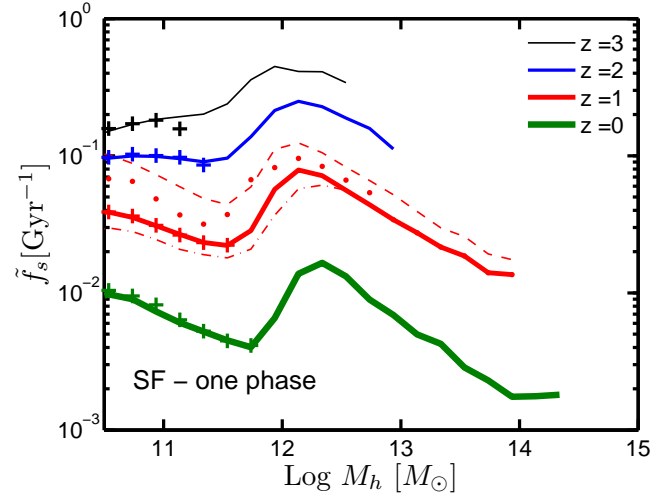


Figure 12. Star-formation efficiencies within the one-phase model, \tilde{f}_s , as defined in Eq. 18. The line-types are the same as in Fig. 3. Plus symbols are showing the average values of \tilde{f}_s using a sample of subhaloes with mass lower than $\sim 10^{12} M_{\odot}$ at $z = 0$, along with all their progenitors.

assume a constant dependence on subhalo mass. As was mentioned above, there are other important differences between the model used here and previous studies. Here the gas mass corresponds to all the gas inside the subhalo, including both cold and hot components, while previous studies have used the cold gas only. In addition, previous models were applied to average main-progenitor histories, while here the model is evolved through the complicated structure of merger-trees.

5.3 Galaxies in the one-phase model

In Fig. 13 (upper left panel) we compare the results of the one-phase SAM discussed above, to the original HYD galaxies. The SAM is based on the efficiency shown in Fig. 12. Although the one-phase model is significantly simpler than our standard model, the results of this model agree well with the HYD, at the same level as in our standard model (there is, however, a small systematic deviation of ~ 0.1 dex that is seen only in low mass galaxies within the one-phase model). We have checked that a similar agreement is obtained at higher redshifts. To summarize, we find the same accuracy in matching the SAM against the HYD when using one, two or three gas phases for each galaxy (the same is true also for the gas components).

The agreement found for the one-phase model proves that the SAM equations are not unique, and that different models can accurately reproduce the same HYD. We will discuss the reasons for this behaviour, and the related implications in section 6.3.

6 MORE TESTS

6.1 Efficiencies based on one galaxy

The efficiencies plotted in Figs. 3-6 have usually a large scatter, when computing the variance over the full population of galaxies within the box. However, we also show that once efficiencies are first averaged over all the progenitors of each $z = 0$ galaxy, the variance decreases significantly. This is shown as the dotted-dashed

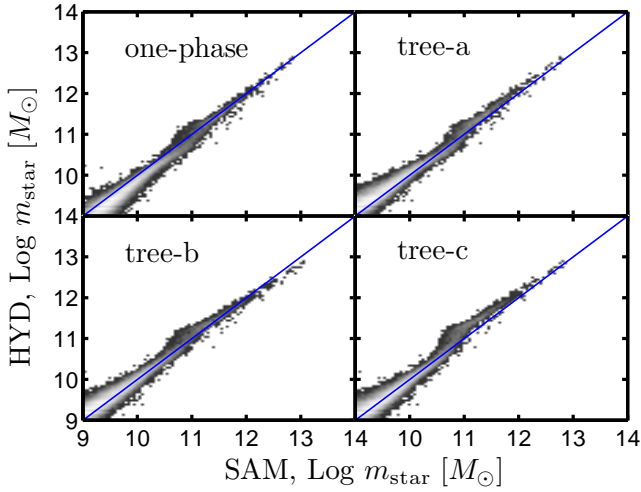


Figure 13. Comparison of the SAM against the HYD, using deviations for individual galaxies. The histograms were derived in the same way as in Fig. 7. Here we plot only stellar masses at $z = 0$. The upper left panel shows the results of the one-phase model (section 5.1). Other panels show a comparison using all galaxies within the box, using SAM efficiencies that are extracted from the history of only *one* massive galaxy at $z = 0$. Each panel is based on efficiencies extracted from a different galaxy, randomly selected.

lines in the efficiency plots. As a result, it should be possible to extract the SAM efficiencies using the history of one massive galaxy within the HYD.

Fig. 13 shows results of various different SAMs. In each model we extracted the SAM efficiencies using only one random massive galaxy within the HYD, along with all its progenitors. The results of these models nicely reproduce the population of the HYD galaxies within the *full* box. This test proves that one can use a single high-resolution zoom simulation in order to extract the net result of the physics of a HYD. Once the efficiencies are known, the SAM can use a large statistics of merger-trees, based on dark-matter only simulations, to explore the same physics as was used in the high-resolution HYD.

At stellar masses of $\sim 10^{11} M_{\odot}$ the agreement between the SAM and HYD is less good. As was discussed in section 4, this might indicate on a larger variation in feedback efficiencies between subhaloes of the same mass.

6.2 The dependence of efficiencies on time-steps and on subhalo mass

The accuracy of the efficiencies discussed here might depend on the number of output snapshots used to extract information from the HYD. For example, since the feedback delay time is 30 Myr after any SF episode, and wind particles are not allowed to form stars for an additional 15 Myr, the snapshot spacing should not go below ~ 50 Myr. To explore the sensitivity of our method to the time between snapshots, we have tested the same method using half of the snapshots in our main run. The full analysis described above was repeated using half of the snapshots, including merger-trees, computation of efficiencies, and running the SAM. We did not find any significant changes in the results, and we conclude that our method is not sensitive to the specific choice of snapshot spacing. It might be that HYDs which include different physical ingredients will show more sensitivity in this respect.

In Fig. 12 we plot in symbols the efficiency, \tilde{f}_s , using a range of low mass subhaloes ($\lesssim 10^{12} M_{\odot}$) within the HYD. We select subhaloes at $z = 0$ and use all their progenitors for computing the average \tilde{f}_s . It is clear that the average \tilde{f}_s for these subhaloes agrees well with the total average within the box. This point allows us to use our method in order to increase the dynamical range of HYDs. Efficiencies for massive subhaloes can in general be extracted using low resolution simulations. On the other hand, efficiencies for low mass subhaloes can be derived using a high-resolution simulation of low mass objects.

6.3 Why do SAM & HYD agree?

In the previous sections we have shown that our SAM agrees quite well with the HYD, even when comparing individual galaxies. This fact seems to be surprising. After all, the HYD follows the dynamics of typically $10^3 - 10^6$ particles within a galaxy, and the rates of cooling, SF, and feedback should be affected by many details within the HYD. For example, metallicity, the abundance of different elements within the gaseous halo, and the gas density profile should all affect the cooling rate strongly (Mo et al. 2010). It is also known that the morphology of the galaxy, and the spatial distribution of cold gas within the disk, should affect the SF rates (McKee & Ostriker 2007). How is it that the simple SAM, based on average efficiencies per subhalo mass and time, can reproduce all these dependencies accurately?

The fact that the simple, one-phase model, provides an accurate match to individual galaxies within the HYD might help us to discover the reasons for the good agreement. We will thus build our arguments using the one-phase model, since it is simpler, and includes an analytic integral solution.

Assume that for a specific galaxy within the HYD, the values of \tilde{f}_s deviate from the average values as adopted by the SAM. From Fig. 12, it looks like deviations between different merger-trees are negligible. This means that within the full history of one galaxy (including all its progenitors), the deviations in \tilde{f}_s with respect to the SAM efficiencies should average to zero. In order to understand how these deviations affect m_{star} we examine the analytic solution presented in Eqs. 19 & 20. As seen from these equations, the mass components of the galaxy depend on integral values, such as the integral of \tilde{f}_s over time. Since the deviations in \tilde{f}_s should be averaged out over time, these deviations do not affect m_{star} much. This is also true if the model is not ideal in the sense that \tilde{f}_s depends on m_{gas} .

The fact that our efficiencies are computed using average values per subhalo mass and time is the other key ingredient for the good match between the SAM and the HYD. Such a method guarantees that on average, the mass of each baryonic component within the SAM will agree with the HYD. Moreover, the scatter between the models should be small because various random processes cancel each other: the SF history of one galaxy is built from different episodes in its history, and the stellar mass is a sum over all these episodes. If each SF event within the HYD includes some random error (with respect to the SAM), the sum of all should have a much smaller scatter. This is the reason why the deviations in SF rates between the HYD and SAM are of the order of 0.5 dex, while the total stellar masses agree much better, to a level of 0.1 dex.

7 SUMMARY AND DISCUSSION

In this work we have developed a method to post-process a hydrodynamical simulation of galaxy formation (HYD), and to extract the simple baryonic laws that shape the evolution of galaxies within it. By using the same laws within a semi-analytic model (SAM), we confirmed that the resulting galaxies in both models remain almost unchanged.

We have used a state-of-the-art HYD, taken from the OWLS project (Schaye et al. 2010). This simulation includes radiative cooling, a galactic wind model for feedback, and a SF recipe that mimics the observed Kennicutt-Schmidt law. On the other hand, we have used a simple SAM, based on the approach presented in Neistein & Weinmann (2010). In this SAM, the processes of accretion, cooling, SF, and feedback, are modeled using efficiencies that depend only on the host subhalo mass and redshift. Although previous studies did not find a good agreement between HYDs and SAMs, our simple SAM can reproduce the results of the advanced HYD at the level of 0.1 dex, when comparing individual galaxies (see Fig. 7). The same level of accuracy is achieved for all redshifts and for various mass components (stars and gas, although the cold gas component shows deviations of ~ 0.2 dex). Statistical properties of galaxies, like the stellar mass function, are accurately reproduced by the SAM as well (see Fig. 10).

We claimed that the main reason for the agreement between the SAM and the HYD is the nature of the differential equations that govern galaxy evolution: Using a simple one-phase model, that can be solved analytically, we show that the mass components depend on the integrals of efficiencies over time, so temporal variations cannot be seen in the total stellar mass of galaxies. On the other hand, instantaneous properties like SF rates, reveal much larger deviations between the SAM and the HYD, at the level of 0.5 dex. The fact that our recipes are matched for the same subhalo mass, implies that objects from the SAM and HYD should agree on average, since the common reference between these models is the merger-tree, based on the subhalo mass.

We have found that satellite galaxies within the HYD experience stripping of hot gas, on a time scale of ~ 3 Gyr. Although we have used only one time-scale for stripping, we found that a more accurate description would demand a time-scale that depends on the satellite mass, and on the infall redshift. In addition, satellite galaxies have different efficiencies of cooling and feedback than central galaxies, a fact that was neglected in this work. Due to the above simplifications made in our model, the agreement between satellite galaxies in the HYD and SAM reaches a value of 0.2 dex at low redshift.

The method presented here is very robust and should work for any hydrodynamical simulation. We have shown that it even works if we assume only one phase of gas within subhaloes. In this highly simplified SAM there are only two processes: smooth accretion, and SF. Nonetheless, the SAM is able to reproduce the same galaxies as in the HYD with the same accuracy as a SAM with more phases of gas (see Fig. 13). This test proves that our method is insensitive to the specific way the SAM equations are written, and that there are many possible models to describe the same simulation.

We have shown that the variance in the baryonic efficiencies is very small, once efficiencies are first averaged over the progenitors of each $z = 0$ galaxy. We have also extracted the SAM efficiencies from the progenitors of one random massive galaxy at $z = 0$. These efficiencies are then able to reproduce the full population of galaxies within the HYD. Consequently, our method can sepa-

rate between baryonic processes and cosmic variance, and can be used to interpret one zoomed hydrodynamical simulation. In a future work, we plan to use the method developed here in order to scan combinations of various implementations of feedback and SF within hydrodynamical simulations.

We have investigated the efficiencies of the baryonic processes within the HYD, showing that this specific simulation deviates from the values adopted by standard SAMs. We have shown that smooth accretion does not always follow dark-matter, and is less efficient for low-mass haloes (see also van de Voort et al. 2011). All the fresh gas falling into subhaloes is either hot or dilute, and cannot form stars. For a given subhalo mass, cooling time-scales are roughly proportional to the cosmic time, with somewhat shorter time-scales at high- z . On the other hand, the efficiency of SF does not change significantly with cosmic time and does not decrease strongly for high-mass haloes. Lastly, the HYD used here does not show noticeable contributions from merger-induced star formation bursts. We hope that these findings can help to bridge the gap between SAMs and HYDs, and will be useful for interpreting various existing models.

ACKNOWLEDGMENTS

We thank the referee for a detailed and constructive report that helped us to improve the paper. We thank Volker Springel for making his code `GADGET` publicly available, and for letting us use the `SUBFIND` code. EN and SK acknowledge funding by the DFG via grant KH-254/2-1. CDV is supported by Marie Curie Reintegration Grant FP7-RG-256573. We acknowledge useful discussions with Till Sawala.

REFERENCES

- Agertz O., Teyssier R., Moore B., 2011, *MNRAS*, 410, 1391
- Benson A. J., Bower R., 2010, *MNRAS*, 405, 1573
- Benson A. J., Pearce F. R., Frenk C. S., Baugh C. M., Jenkins A., 2001, *MNRAS*, 320, 261
- Bouché N., et al., 2010, *ApJ*, 718, 1001
- Bower R. G., Benson A. J., Malbon R., Helly J. C., Frenk C. S., Baugh C. M., Cole S., Lacey C. G., 2006, *MNRAS*, 370, 645
- Cattaneo A., et al., 2007, *MNRAS*, 377, 63
- Cole S., 1991, *ApJ*, 367, 45
- Cole S., Lacey C. G., Baugh C. M., Frenk C. S., 2000, *MNRAS*, 319, 168
- Conroy C., et al., 2007, *ApJ*, 654, 153
- Cox T. J., Jonsson P., Somerville R. S., Primack J. R., Dekel A., 2008, *MNRAS*, 384, 386
- Crain R. A., et al., 2009, *MNRAS*, 399, 1773
- Crain R. A., McCarthy I. G., Frenk C. S., Theuns T., Schaye J., 2010, *MNRAS*, 407, 1403
- Croton D. J., et al., 2006, *MNRAS*, 365, 11
- Dalla Vecchia C., Schaye J., 2008, *MNRAS*, 387, 1431
- Davé R., Oppenheimer B. D., Finlator K., 2011, *MNRAS*, 415, 11
- Davis M., Efstathiou G., Frenk C. S., White S. D. M., 1985, *ApJ*, 292, 371
- De Lucia G., Blaizot J., 2007, *MNRAS*, 375, 2
- De Lucia G., Boylan-Kolchin M., Benson A. J., Fontanot F., Monaco P., 2010, *MNRAS*, 406, 1533
- Dekel A., et al., 2009, *Nature*, 457, 451
- Dekel A., Silk J., 1986, *ApJ*, 303, 39

- Dolag K., Borgani S., Murante G., Springel V., 2009, MNRAS, 399, 497
- Dutton A. A., van den Bosch F. C., 2009, MNRAS, 396, 141
- Fu J., Guo Q., Kauffmann G., Krumholz M. R., 2010, MNRAS, 409, 515
- Gao L., Springel V., White S. D. M., 2005, MNRAS, 363, L66
- Governato F., Gardner J. P., Stadel J., Quinn T., Lake G., 1999, AJ, 117, 1651
- Guo Q., et al., 2011, MNRAS, 413, 101
- Haas M. R., 2010, PhD thesis, Ph. D. thesis, University of Leiden (2010)
- Helly J. C., Cole S., Frenk C. S., Baugh C. M., Benson A., Lacey C., Pearce F. R., 2003, MNRAS, 338, 913
- Hernquist L., Springel V., 2003, MNRAS, 341, 1253
- Hirschmann M., Naab T., Somerville R., Burkert A., Oser L., 2011, ArXiv e-prints, 1104.1626
- Hopkins P. F., et al., 2010, ApJ, 724, 915
- Katz N., Weinberg D. H., Hernquist L., 1996, ApJS, 105, 19
- Kereš D., Katz N., Fardal M., Davé R., Weinberg D. H., 2009, MNRAS, 395, 160
- Kereš D., Katz N., Weinberg D. H., Davé R., 2005, MNRAS, 363, 2
- Khochfar S., et al., 2011, ArXiv e-prints, 1107.5059
- Khochfar S., Ostriker J. P., 2008, ApJ, 680, 54
- Khochfar S., Silk J., 2006, MNRAS, 370, 902
- Khochfar S., Silk J., 2009, ApJ, 700, L21
- Khochfar S., Silk J., 2011, MNRAS, 410, L42
- Komatsu E., et al., 2009, ApJS, 180, 330
- Krumholz M. R., Dekel A., 2011, ArXiv e-prints, 1106.0301
- Lacey C., Cole S., 1993, MNRAS, 262, 627
- Lotz J. M., et al., 2008, ApJ, 672, 177
- Lu Y., Kereš D., Katz N., Mo H. J., Fardal M., Weinberg M. D., 2011, MNRAS, pp 1035–
- McCarthy I. G., Babul A., Bower R. G., Balogh M. L., 2008, MNRAS, 386, 1309
- McCarthy I. G., Schaye J., Bower R. G., Ponman T. J., Booth C. M., Dalla Vecchia C., Springel V., 2011, MNRAS, 412, 1965
- McKee C. F., Ostriker E. C., 2007, ARA&A, 45, 565
- Mihos J. C., Hernquist L., 1994, ApJ, 431, L9
- Mo H., van den Bosch F. C., White S., 2010, Galaxy Formation and Evolution
- Monaco P., Fontanot F., Taffoni G., 2007, MNRAS, 375, 1189
- Monaco P., Murante G., Borgani S., Fontanot F., 2006, ApJ, 652, L89
- Moster B. P., Macciò A. V., Somerville R. S., Naab T., Cox T. J., 2011, MNRAS, pp 1064–
- Neistein E., Weinmann S. M., 2010, MNRAS, 405, 2717
- Press W. H., Schechter P., 1974, ApJ, 187, 425
- Purcell C. W., Bullock J. S., Zentner A. R., 2007, ApJ, 666, 20
- Rasera Y., Teyssier R., 2006, A&A, 445, 1
- Rees M. J., Ostriker J. P., 1977, MNRAS, 179, 541
- Saintonge A., et al., 2011, MNRAS, 415, 61
- Sales L. V., Navarro J. F., Schaye J., Dalla Vecchia C., Springel V., Booth C. M., 2010, MNRAS, 409, 1541
- Saro A., De Lucia G., Borgani S., Dolag K., 2010, MNRAS, 406, 729
- Scannapieco C., White S. D. M., Springel V., Tissera P. B., 2009, MNRAS, 396, 696
- Schaye J., Dalla Vecchia C., 2008, MNRAS, 383, 1210
- Schaye J., et al., 2010, MNRAS, 402, 1536
- Schiminovich D., et al., 2010, MNRAS, 408, 919
- Silk J., 1977, ApJ, 211, 638
- Somerville R. S., 2002, ApJ, 572, L23
- Somerville R. S., Hopkins P. F., Cox T. J., Robertson B. E., Hernquist L., 2008, MNRAS, 391, 481
- Somerville R. S., Primack J. R., Faber S. M., 2001, MNRAS, 320, 504
- Springel V., Hernquist L., 2003, MNRAS, 339, 289
- Springel V., White S. D. M., Tormen G., Kauffmann G., 2001, MNRAS, 328, 726
- Stringer M. J., Brooks A. M., Benson A. J., Governato F., 2010, MNRAS, 407, 632
- van de Voort F., Schaye J., Booth C. M., Haas M. R., Dalla Vecchia C., 2011, MNRAS, 414, 2458
- Viola M., Monaco P., Borgani S., Murante G., Tornatore L., 2008, MNRAS, 383, 777
- Wang L., Weinmann S. M., Neistein E., 2011, ArXiv e-prints, 1107.4419
- Weinmann S. M., Kauffmann G., von der Linden A., De Lucia G., 2010, MNRAS, 406, 2249
- Weinmann S. M., Neistein E., Dekel A., 2011, ArXiv e-prints, 1103.3011
- Wetzel A. R., 2011, MNRAS, 412, 49
- White S. D. M., Frenk C. S., 1991, ApJ, 379, 52
- White S. D. M., Rees M. J., 1978, MNRAS, 183, 341
- Wiersma R. P. C., Schaye J., Smith B. D., 2009, MNRAS, 393, 99
- Wiersma R. P. C., Schaye J., Theuns T., 2011, MNRAS, 415, 353
- Wiersma R. P. C., Schaye J., Theuns T., Dalla Vecchia C., Tornatore L., 2009, MNRAS, 399, 574
- Yang X., Mo H. J., van den Bosch F. C., 2009, ApJ, 693, 830
- Yoshida N., Stoehr F., Springel V., White S. D. M., 2002, MNRAS, 335, 762

APPENDIX A: MORE EFFICIENCIES

In this section we plot additional efficiency values that were extracted from the HYD. In Fig. A1 we plot the smooth accretion, when stripping is allowed for central galaxies. These accretion rates are very different from our standard model (Fig. 3), proving that stripping occurs often in low mass haloes.

In Fig. A2 we show the cooling and feedback efficiencies when we use an additional gas phase, m_{ejc} to describe the ejected gas. Here f_c describes the transition from m_{hot} to m_{cold} only, and is normalized by m_{hot} . Feedback is defined as the total heated gas, including all gas particles that started within m_{cold} and ended within m_{hot} or m_{ejc} .

The efficiencies plotted in Figs. 3-6 use a fixed particle mass, and do not account for mass loss due to SN and stellar winds. Although these efficiencies were treated self-consistently in the main body of this work, they might deviate from the true efficiencies, computed with the proper particle mass. In Figs. A3 & A4 we plot the true efficiencies. These are very similar to the values used before, but show some small differences in the overall normalization.

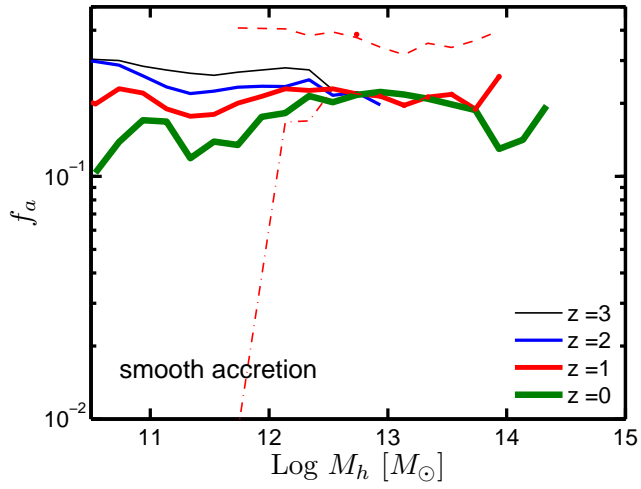


Figure A1. The smooth accretion rate of baryons as derived from the hydrodynamical simulation, using a model in which stripping of hot gas follows the dark-matter stripping. The definitions of line-types are the same as in Fig. 3.

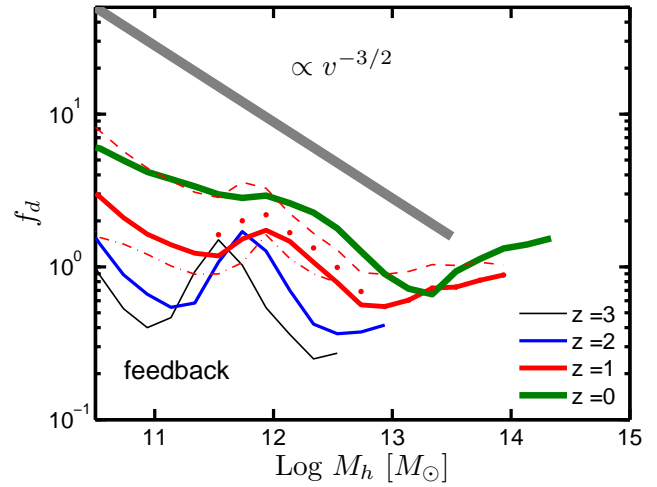
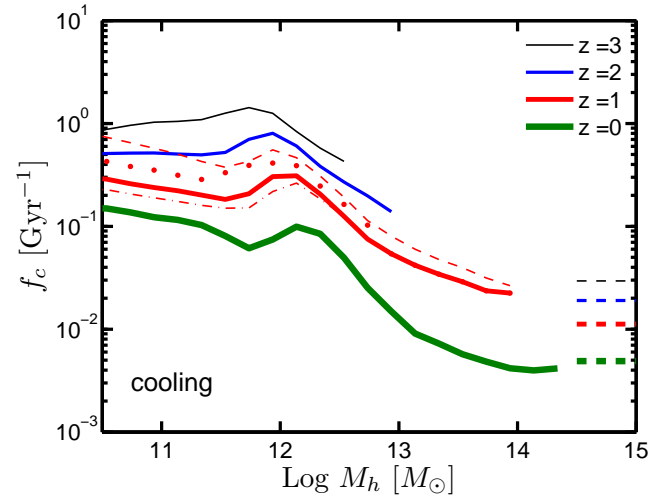


Figure A2. The cooling and feedback efficiencies within the HYD, using a separate ejection phase. The definitions of line-types are the same as in Fig. 3.

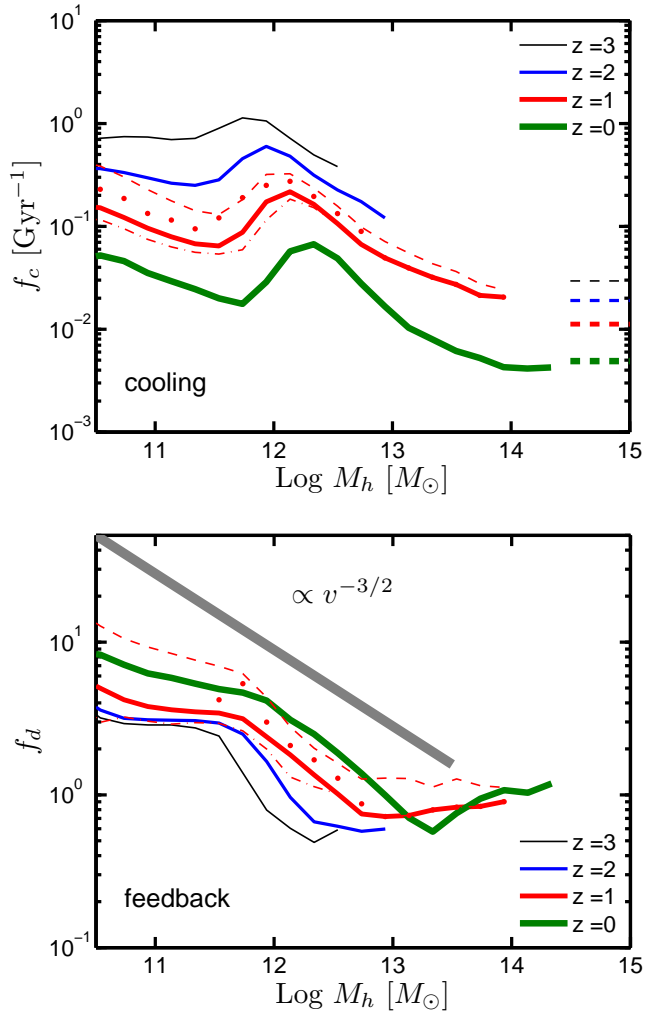


Figure A3. The cooling and feedback efficiencies using the proper mass for each particle within the HYD. The definitions of line-types are the same as in Fig. 3.

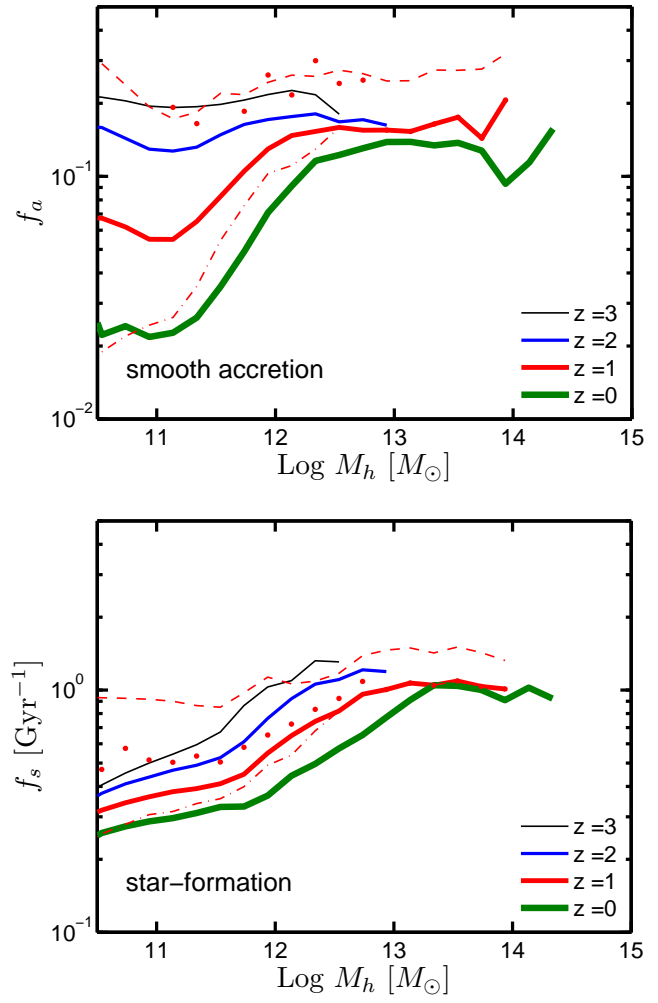


Figure A4. The accretion and SF efficiencies using the proper mass for each particle within the HYD. The definitions of line-types are the same as in Fig. 3.